AGU PUBLICATIONS

Water Resources Research

RESEARCH ARTICLE

10.1002/2016WR020233

Key Points:

- *n* and *f* coefficients in fully bedrock, partial-cover and fully alluvial reaches all vary greatly with discharge but differ between reaches
- Flow resistance of partly covered bedrock decreases with discharge and submergence in a similar way to coarse-bed alluvial channels
- Resistance in the sediment-free bedrock reach increases at high discharges because rock walls are rougher than bed

Correspondence to:
R. I. Ferguson
r.i.ferguson@durham.ac.uk

Citation:
Ferguson, R. I., B. P. Sharma, R. J. Hardy, R. A. Hodge, and J. Warburton (2017), Flow resistance and hydraulic geometry in contrasting reaches of a bedrock channel, *Water Resour. Res.*, *53*, 2278–2293, doi:10.1002/2016WR020233.

Received 5 DEC 2016
Accepted 22 FEB 2017
Accepted article online 2 MAR 2017
Published online 22 MAR 2017

© 2017. American Geophysical Union. All Rights Reserved.

Flow resistance and hydraulic geometry in contrasting reaches of a bedrock channel

R. I. Ferguson[1], B. P. Sharma[1], R. J. Hardy[1], R. A. Hodge[1], and J. Warburton[1]

[1]Department of Geography, Durham University, Durham, UK

Abstract Assumptions about flow resistance in bedrock channels have to be made for mechanistic modeling of river incision, paleoflood estimation, flood routing, and river engineering. Field data on bedrock flow resistance are very limited and calculations generally use standard alluvial-river assumptions such as a fixed value of Manning's *n*. To help inform future work, we measured how depth, velocity, and flow resistance vary with discharge in four short reaches of a small bedrock channel, one with an entirely rock bed and the others with 20–70% sediment cover, and in the alluvial channel immediately upstream. As discharge and submergence increase in each of the partly or fully alluvial reaches there is a rapid increase in velocity and a strong decline in both *n* and the Darcy-Weisbach friction factor *f*. The bare-rock reach follows a similar trend from low to medium discharge but has increasing resistance at higher discharges because of the macroroughness of its rock walls. Flow resistance at a given discharge differs considerably between reaches and is highest where the partial sediment cover is coarsest and most extensive. Apart from the effect of rough rock walls, the flow resistance trends are qualitatively consistent with logarithmic and variable-power equations and with nondimensional hydraulic geometry, but quantitative agreement using sediment D_{84} as the roughness height is imperfect.

1. Introduction

Scientific investigation of what controls the depth and velocity of a river began in the 1700s and there is now a large and continually growing literature on the topic, including recent reviews of flow resistance [*Ferguson*, 2013; *Powell*, 2015] and hydraulic geometry [*Gleason*, 2014]. Almost all of this literature refers to natural or engineered alluvial rivers. In contrast, very little is known about the bulk hydraulics of bedrock rivers and in particular their flow resistance behavior.

One reason for the scarcity of information on bedrock channel hydraulics may be the difficulty of making measurements, especially in high flows. Another may be a perceived lack of practical importance. In unconfined alluvial rivers, a knowledge of flow resistance helps assess flood risk, but most bedrock channels are incised so that water depth is unimportant from that point of view. Flow resistance in bedrock channels is, however, of interest in at least two contexts: mechanistic modeling of river incision and landscape evolution, and paleoflood estimation from depositional traces in bedrock gorges. It may also be relevant to flood routing and ecological assessment in some catchments, and to river engineering projects. Researchers or practitioners working on any of these topics have to make assumptions about flow resistance, and in the near absence of relevant data they have generally adopted standard formulae from the river engineering literature. Whether these are appropriate is open to question. Bedrock channels are usually steep and almost always contain a partial cover of coarse sediment. Geomorphologists investigating the hydraulics of alluvial channels with coarse beds have found that few standard flow resistance relations work well and have proposed alternatives [e.g., *Ferguson*, 2007; *Rickenmann and Recking*, 2011]. These findings may be relevant to bedrock channels.

The knowledge gap that exists about the bulk hydraulics of bedrock channels, and the suspicion that standard alluvial flow resistance relations may be unsuitable, motivated us to make field measurements in a small bedrock channel to investigate its bulk hydraulics. In this paper, we report how reach-averaged flow resistance varies with water discharge in contrasting short reaches of the study stream and how, at any given discharge, flow resistance differs between reaches with a fully exposed rock bed, partly covered rock bed, or fully alluvial bed. We discuss similarities and differences between the observed flow resistance

behavior and hydraulic geometry in this stream and in coarse alluvial channels, and show that the observed behaviour differs from what has generally been assumed in bedrock incision models and by paleohydrologists.

2. Background

Before describing our field investigation, we outline the basics of reach-averaged flow resistance and hydraulic geometry and note the assumptions made about flow resistance by incision modellers and paleohydrologists. We also summarize previous field investigations of bedrock flow resistance and recent advances in predicting flow resistance over coarse alluvial beds.

2.1. Flow Resistance and Hydraulic Geometry

As discharge (Q) increases in a channel, so do the wetted width (w), mean depth and hydraulic radius (d and R), and mean velocity (v). The changes in w, d, and v are often represented by power laws in what *Leopold and Maddock* [1953] termed the at-a-station hydraulic geometry (AHG) of a river. The AHG of a particular channel depends on its geometry and flow resistance behavior [*Ferguson*, 1986; *Dingman*, 2007], since cross-section shape determines how width changes with depth and flow resistance determines how velocity changes with depth.

Flow resistance is traditionally represented in one of three ways. The commonest is a fixed value of n in the Manning equation

$$v = R^{2/3} S^{1/2} / n \tag{1}$$

where S denotes channel slope. The two main alternatives are a fixed value of the Darcy-Weisbach friction factor f in

$$v = (8gRS/f)^{1/2} \tag{2}$$

where g is the gravity acceleration, or a fixed roughness height k in the logarithmic resistance relation obtained by integrating the law of the wall:

$$v/(gRS)^{1/2} = (8/f)^{1/2} = 2.5\ \ln(aR/k) \tag{3}$$

where α is a shape factor in the range 11–13 [*Keulegan*, 1932; *Hey*, 1979]. In a given cross section, the rate of change of depth with discharge is progressively greater for fixed k, fixed n, and fixed f.

Unless flow measurements have been made at one or more discharges, the value of the preferred roughness parameter must be assigned on the basis of visual or measured characteristics of the channel. Fixed values of n are often estimated from tables in textbooks or images of channels with different measured n [e.g., *Chow*, 1959; *Barnes*, 1967], or assumed proportional to $D^{1/6}$ where D is a representative bed grain diameter [*Strickler*, 1923]. The roughness height k in equation (3) is generally estimated from D_{84} or D_{90} (84th or 90th percentile of the grain size distribution), but the standard deviation of bed elevation (s_z hereafter) is also used [e.g., *Smart et al*., 2002; *Aberle and Smart*, 2003] and has the advantage of applicability to exposed bedrock [*Inoue et al*., 2014].

2.2. Hydraulic Assumptions Made in Bedrock Incision Models

The incision of bedrock channels constrains landscape evolution in many elevated and/or tectonically active parts of the continents. Almost all landscape evolution models from *Howard* [1994] onwards have assumed that local incision rate depends on bed shear stress ($\tau = \rho gRS$ where ρ denotes water density). Such models calculate shear stress from local discharge and slope using a flow resistance law and the numerical value of its roughness parameter. The same is true of most mechanistic models proposed for specific incision processes such as abrasion and plucking [e.g., *Lamb et al*., 2008; *Chatanantavet and Parker*, 2009], for the evolution of bedrock channel geometry [e.g., *Turowski et al*., 2008], and for the mutual adjustment of sediment cover and bed load transport rate in bedrock reaches [e.g., *Johnson*, 2014; *Inoue at al*., 2016].

Some researchers have assumed a fixed value of f [e.g., *Whipple and Tucker*, 1999; *Chatanantavet and Parker*, 2009; *Zhang et al*., 2015], others have assumed a constant value of Manning's n [e.g., *Howard*, 1994; *Turowski et al*., 2007, 2008, 2009], and *Lague et al*. [2005] considered both possibilities. *Johnson* [2014] used an area-

weighted Manning-Strickler calculation with $n \propto k^{1/6}$ but different values of k for bare rock and sediment cover, and *Chatanantavet and Parker* [2008] used this type of resistance law to back-calculate k from measurements in artificial "bedrock" channels. Logarithmic resistance laws equivalent to equation (3), which implies a decrease in both f and n as discharge and depth increase, were used by *Lamb et al*. [2008] and *Nelson and Seminara* [2012] in models and by *Inoue et al*. [2014] to calculate the hydraulic roughness height of a bedrock channel. Different assumptions about flow resistance would affect the calculated shear stresses in these various models, and thus their quantitative predictions about the topics of primary interest.

2.3. Hydraulic Assumptions for Paleoflood Estimation in Bedrock Gorges

Paleoflood discharges estimated from sedimentary traces in bedrock gorges are used to reconstruct individual extreme events and constrain regional flood magnitude-frequency curves [*O'Connor and Webb*, 1988; *Benito and Thorndycraft*, 2005]. The discharge in a step-backwater flow calculation is adjusted to match as closely as possible the reconstructed peak water-surface elevations at a series of surveyed cross sections. The calculation requires a flow resistance equation and a specific value of its roughness parameter at each section. The near-universal practice is to use the Manning equation and a stage-invariant value of n at each section, often the same for all sections but sometimes spatially variable. Few papers on paleoflood estimation explain how n was specified, and *Miller and Cluer* [1998] regarded the choice of value as "a significant unresolved question . . . [since] . . . roughness is expected to decrease with increasing depth of flow."

For any given representation of the channel geometry a higher/lower value of n gives a lower/higher estimate of the paleoflood discharge. *Wohl* [1998] compared paleoflood estimates for five gorges using four alternatives for n: tabulated values, visual estimates, *Jarrett's* [1984] empirical equation, and n derived by using the log law with $k = D_{84}$. The highest estimate of Q in each river exceeded the lowest by 33–108%, implying a typical uncertainty in Q of around $\pm$20%. As *Wohl* [1998] noted, this is no higher than other uncertainties involved in estimating flood frequency curves using paleoflood estimates, but it does suggest a need for measurements of flow resistance in bedrock gorges to help constrain assumptions made in paleoflood studies.

2.4. Field Investigations of Bedrock Flow Resistance

There have been few previous attempts to measure flow resistance in bedrock channels, and some of them were restricted to a single discharge. Studies at more than one discharge all show some reduction in n and/or f at higher stages [*Heritage et al*., 2004; *Kidson et al*., 2006; *Richardson and Carling*, 2006; *Siddiqui and Robert*, 2010], though *Richardson and Carling* [2006] found that n became almost constant at high discharges.

Comparisons between measured flow resistance and small-scale topographic roughness are also rare. *Chatanantavet and Parker* [2008] did not find a consistent relation for different artificial "bedrock" surfaces, but *Inoue et al*. [2014] found that the log-law k of natural bedrock in an artificially excavated channel was approximately equal to its topographic roughness as quantified by s_z. *Goode and Wohl* [2010] calibrated spatially distributed n values to water-surface profiles measured during a controlled reservoir release in a bedrock river with 50% sediment cover, and found higher mean n values in a reach with transverse rock ribs than in reaches with oblique or flow-parallel ribs.

2.5. Flow Resistance in Alluvial Streams With Coarse Beds

The Manning and logarithmic resistance relations (equations (1) and (3)) are good representations of grain resistance in deep gravel-bed rivers where R/D is $>$10 or even $>$100. In steep cobble/boulder channels, however, the relative submergence is usually well below 10 and sometimes of order 1. The distinction between grain and form resistance now becomes blurred, with individual grains exerting significant form drag, and much momentum is dissipated in wakes, standing waves, and spill over any steps or logs [*David et al*., 2011; *D'Agostino and Michelini*, 2015].

It is therefore natural to ask how resistance varies with submergence. Analyses of large data compilations [*Ferguson*, 2007; *Rickenmann and Recking*, 2011; *Ferguson*, 2013] have shown that the relation between $(8/f)^{1/2}$ and R/D_{84}, or any similar measure of relative submergence, does not follow a single power law over the full range of natural conditions. The Manning equation with $n \propto D^{1/6}$ implies $(8/f)^{1/2} \propto (R/D)^{1/6}$, which matches the general trend only for deep flows. As R/D drops toward 1 the trend becomes much steeper. The logarithmic resistance equation reproduces this general pattern, but only fits field data if k is increased to 3–4 times D_{84} [e.g., *Hey*, 1979; *Ferguson*, 2007].

Some alternative resistance relations have been proposed specifically for shallow flows, and others for the full range of submergence including very shallow flows. *Rickenmann* [1991] and *Aberle and Smart* [2003] found that resistance in steep flumes with coarse beds was well described by the dimensionally consistent AHG relation

$$v \propto g^{0.2} S^{0.2} q^{0.6} / k^{0.4} \tag{4}$$

where $q = Q/w$. *Rickenmann* [1991] represented the roughness height k in this equation by D_{90} whereas *Aberle and Smart* [2003] used s_z. *Ferguson* [2007] noted that equation (4) is equivalent to $(8/f)^{1/2} \propto R/k$ and proposed a variable-power equation (VPE) with this as its shallow-flow asymptote, conceptually representing form drag, and Manning-Strickler as the deep-flow asymptote, representing grain friction:

$$(8/f)^{1/2} = a_1 a_2 (R/D_{84}) / \left[a_1{}^2 + a_2{}^2 (R/D_{84})^{5/3} \right]^{1/2} \tag{5}$$

Ferguson [2007], *Rickenmann and Recking* [2011], and *Ferguson* [2013] all found that this gave a better overall fit than any previous equation to large data sets extending from very shallow to moderately deep flows. The asymptotes of the VPE can also be written in nondimensional form as $v^{**} \propto q^{**0.6}$ for shallow flows and $v^{**} \propto q^{**0.4}$ for deep flows, where $v^{**} = v/(gSD_{84})^{1/2}$ and $q^{**} = q/(gSD_{84}^3)^{1/2}$. *Rickenmann and Recking* [2011] devised a continuous function linking these asymptotic expressions for v^{**} and showed that this AHG-style version of the VPE gave the best fit of all to their data compilation.

3. Study Site

Fieldwork was carried out in 2013–2015 as part of an investigation of bed load transport [*Ferguson et al.*, 2017] in a short reach of Trout Beck, a small river in the Pennine Hills of northern England (54°41.5′N, 2°23.3′W, 550 m above sea level). The river flows approximately along the dip of very gently tilted Carboniferous sedimentary strata which are thinly covered in most places by glacial deposits and/or peat. Its channel is mostly alluvial with a bankfull width of 10–15 m, but these alluvial segments are separated by short bedrock segments with small waterfalls and narrow gorges where the river has cut through resistant bands of massive limestone.

The 0.4 km long study site is at one such location. It begins near the end of one alluvial segment and extends into, along and out of a limestone gorge to the start of the next alluvial segment. There is a 1.5 m high waterfall at the head of the gorge. For the next 85 m, the channel is 5–7 m wide between bedrock side walls with angular protrusions and reentrants. It contains no sediment apart from very small (~0.1 m^2) patches of gravel in wall re-entrants, and its rock bed is very smooth apart from a shallow inner channel, small scallops and downstream-facing steps. Along the remaining 160 m the channel is slightly wider (7–10 m) and the rock bed has a partial sediment cover, varying locally from 10% to 80%. The overall gradient is 0.020 but with local departures from that average. Sediment, where present, consists of cobbles, boulders, and gravel. The channel is undivided and only slightly sinuous. It does not contain any woody debris and is not steep enough to have well-defined steps and pools, but parts of it contain large boulders (maximum diameter 1.1 m).

We estimated bulk hydraulic variables over a wide range of discharge in each of five short (24–28 m) reaches which we label F1–F5 in downstream order. Their character is summarized in Table 1 and illustrated in Figure 1. Reach F1 is in the upstream alluvial channel and provides a comparison with the bedrock reaches F2–F5, which were selected as being internally homogeneous but differing in slope and the amount

Table 1. Summary Characteristics of Reaches

Reach	Bank Type	Sediment Cover (%)	Sediment D_{50} (mm)	Sediment D_{84} (mm)	Boulder Density (% of Bed Area)	Bankfull Width (m)	Water-Surface Slope[a]
F1	Alluvial	100	36	116	0	11	0.010
F2	Rock	Negligible			0	6	0.021–0.024
F3	Rock	70	84	190	11	7	0.021–0.022
F4	Rock	70	68	190	4	7	0.007–0.008
F5	Alluvial	20	64	140	<1	10	0.021–0.024

[a]Range shown is for water discharges from 1.6 to 9.4 m^3 s^{-1}.

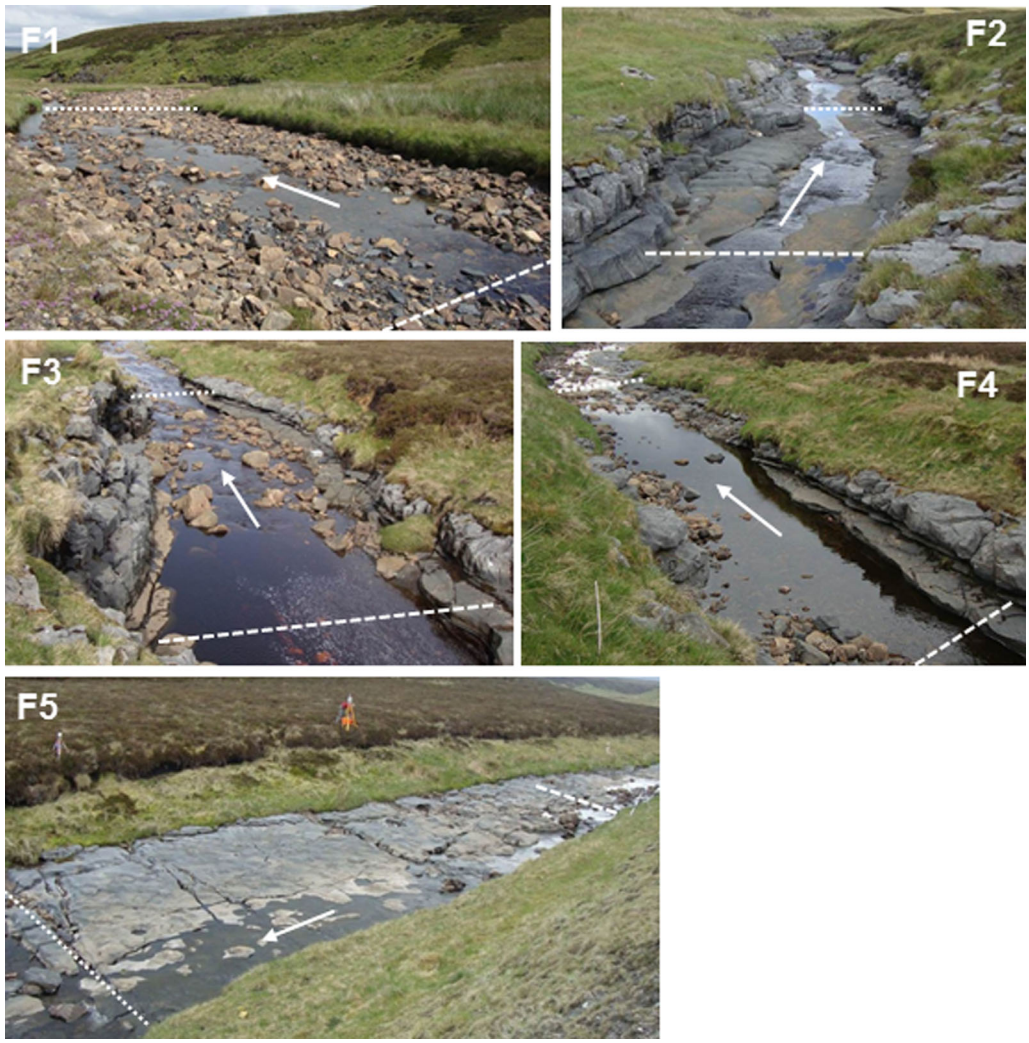

Figure 1. Reaches F1–F5 of Trout Beck at low flow ($Q < 0.1$ m^3 s^{-1}). Arrows show flow direction.

and calibre of sediment cover. F2 is in the part of the bedrock gorge with negligible sediment cover. F3 and F4 are also in the gorge but have a 70% cover of notably coarse sediment. They differ in that F4 is less steep than F3 and contains fewer boulders. F5 has alluvial banks but its bed is mainly rock and what sediment it contains is finer than in F3 and F4, with very few boulders. The upstream alluvial channel (F1) is less steep than most of the gorge and its bed sediment is finer than the partial cover in F3–F5.

Trout Beck is gauged by the Environment Agency (EA) 0.6 km downstream from the study site. However, the drainage area above the study site is only 62% of that at the EA gauge because a substantial tributary joins just before the gauging structure. The tributary catchment has a lower maximum elevation (760 m compared to 848 m) but the same geology, superficial cover, and vegetation, so as explained in detail below we assume hydrological similarity to help estimate discharges in the study reach. The regime is flashy, with a lag between rainfall and runoff peaks of less than 3 h in well-defined events. Over the 24 year period during which 15 min data have been recorded at the EA gauge the mean discharge there is 0.62 m^3 s^{-1} and the mean annual flood is 17.2 m^3 s^{-1}, suggesting a mean annual flood of ~11 m^3 s^{-1} at the study site. The highest EA discharge during the study period was 14.2 m^3 s^{-1}.

4. Methods

The morphology of each reach was surveyed, including the limits of sediment cover. Sediment size distributions were obtained by pebble counts in small (~10 m^2) areas of homogeneous cover and the locations of

clasts with a visible axis exceeding 256 mm were mapped so that boulder density could be quantified. The topographic roughness of exposed bedrock was quantified in one reach. Discharges on different occasions were obtained by direct measurement or from the discharge at the EA gauging station. Water-surface profiles were measured at low to moderate flows and estimated using stage logger data for a range of higher flows, allowing flow resistance and AHG to be calculated for a wide range of discharges in each reach.

4.1. Stage-Discharge Rating Curves

Eight current-meter and 52 salt-dilution discharge measurements were made in low-flow and flood-recession conditions ($Q = 0.05$–2.1 m^3 s^{-1}). They gave a well-defined rating curve at a local stage board after omitting a few anomalous dilution gaugings affected by dead zones. Because of the flashiness of the stream we were seldom on site during high discharges and safety considerations precluded direct flow measurements on those occasions. A linear regression of measured discharges on those at the EA gauge at the same time has a slope of 0.65 ± 0.02 (95% confidence). This is very close to the catchment area ratio of 0.62. On this basis, we assume that discharges higher than 2.1 m^3 s^{-1} at the study site are on average 65% of the corresponding EA discharge during flood events caused by frontal rainfall, though possibly much more or much less in floods generated by localized convective storms in summer.

Continuous stage records were obtained using pressure transducers at the start of reach F1, the end of reach F5, and five intermediate locations. We constructed stage-discharge rating curves for each location by noting the times when several different EA discharge values were passed on the rising and falling limbs of each of six large frontal-rainfall flood events in 2013–2014, multiplying the EA discharges by 0.65 to obtain an estimated local discharge Q, and matching this discharge to the stage h at each pressure transducer. During floods the discharge changes fairly rapidly so we allowed for travel time at $\sim$1 m s^{-1} by matching the EA discharge to our stage readings 15 min previously. We then added these high-flow h, Q pairs to the measured low-flow pairs and fitted power laws between Q and h-h_0 by least squares. Here h_0 is a depth offset that depends on the position of the transducer within the cross section. The seven rating curves are shown in Figure 2. The steepest curves are for the narrow rock-walled sections (PT4 and PT5) and the least

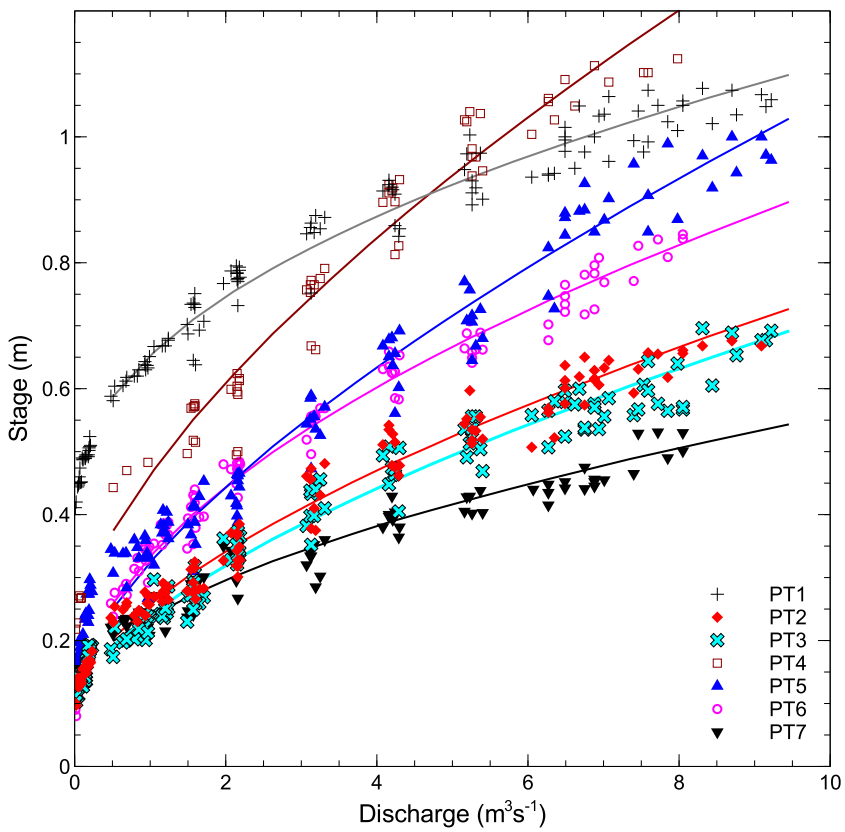

Figure 2. Stage-discharge rating curves for the seven pressure transducers, labeled PT1–PT7 in downstream order.

steep curves are for the widest sections (PT1 and PT7). There is scatter around the curves in the Q direction because of errors in the salt dilution measurements and temporary departures from the 0.65 discharge ratio during floods, but the correlations are very strong (r^2 0.96–0.98) and the root-mean-square error in predicting h from the scaled EA Q is small: 0.02–0.05 m, which corresponds to only 4–6% of the measured increase in stage from low flow to flood conditions.

4.2. Reach-Averaged Hydraulic Variables

We used differential Global Positioning System (dGPS) methods with a nominal elevation precision of $\pm$0.02 m to survey 7–10 almost equally spaced cross sections within each reach, and estimated the water-surface elevation at 5–8 directly measured discharges per cross section by interpolation from water-surface profiles measured using 20–30 dGPS readings along one side of the reach. A significant lateral water-surface slope is unlikely since the reaches are almost straight and do not contain diagonal bed steps. This allowed calculation of the wetted width, area (A) and perimeter (P) at each discharge in each cross section. From these, we calculated $R = A/P$, $d = A/w$, and $v = Q/A$ for each section, then reach-average hydraulic radius as $\langle A\rangle/\langle P\rangle$, reach-average velocity as $Q/\langle A\rangle$, and reach-average depth as $\langle A\rangle/\langle w\rangle$, where angle brackets denote averages over the 7–10 sections in the reach. The water-surface profile also gave the mean water-surface slope (S_w) at each discharge, from which the energy slope S_e was obtained by adjusting for the difference between the velocity heads at the first and last cross sections. Finally, reach-average values of the resistance coefficients f and n at each discharge were calculated by substituting reach-average v, R, and S_e in equations (1) and (2).

To extend these directly measured results for low to moderate discharges, we estimated water-surface profiles in each reach at 12 progressively higher discharges from 1.6 to 9.4 $m^3\ s^{-1}$ (the highest flow during the study period). This was done by progressively raising the highest measured water-surface elevation at each cross section within each reach using the rating curves for the nearest pressure transducer upstream and the nearest pressure transducer downstream. The increment at a particular cross section was calculated as a distance-weighted average of the stage increments at the two pressure transducers:

$$\Delta h = [(\Delta x_2 \Delta h_1 + \Delta x_1 \Delta h_2)/(\Delta x_1 + \Delta x_2) \tag{6}$$

Here Δh is the estimated increase in stage at the cross section of interest, Δh_1 and Δh_2 are the increases at the upstream and downstream pressure transducers as given by the rating curves in Figure 2, and Δx_1 and Δx_2 are the distances from the cross section of interest to those transducers. This weights the calculation toward the nearer transducer and allows for any change in water-surface slope. S_w and S_e increased slightly with discharge in F2, F4, and F5 but stayed almost constant in F1 (Table 1), while in F3 S_w increased slightly but S_e decreased slightly. Finally, for each discharge we calculated cross-section and reach-average flow properties in the same way as described above for measured water-surface profiles.

Extrapolating water-surface profiles in this way is subject to several uncertainties, but an error analysis suggests they do not significantly affect the key results. The estimated profile for a particular discharge could be too high or low if the highest measured water-surface profile was inaccurate, but any such error is unlikely to exceed $\pm$0.02 m and the profiles at all discharges would be displaced by the same amount so that trends in how R and v vary with Q would not be affected. As previously noted there is a root-mean-square scatter of 0.02–0.05 m around the rating curves for the pressure transducers, but the change in stage from one discharge to the next in equation (6) is based on the smooth fitted curves, not individual readings. Based on the scatter around the rating curves and the dGPS precision we calculate that reach water-surface slopes expressed as m m^{-1} are accurate to $\pm$0.002 in F2 and $\pm$0.001 in the other reaches; this is a relative error of only 3–7%. Another source of uncertainty is any change in the shape of the water-surface profiles as discharge increases; in particular, stepped low-flow profiles over irregular beds tend to become straighter as discharge rises. But comparison of the measured profiles at different discharges shows that much of this change had already happened by the highest measured discharges; moreover, any further straightening of the profile at higher discharges would increase water-surface elevation at some cross sections but lower it at others, with little or no effect on reach-averaged R and v. Finally, estimates of reach-average R (and therefore v) are subject to uncertainty because of longitudinal variation in cross-section geometry. Averaging over 7–10 sections keeps this uncertainty to an acceptable level: the standard error of reach-average R at moderate to high flows is only 0.01–0.03 m, or 2–7%.

4.3. Topographic Roughness of Exposed Bedrock

When comparing our results with published flow resistance equations later in the paper (section 6.1) the question arises of what roughness height to use. We use the local sediment D_{84} in the fully alluvial reach F1, and also as one option for the reaches with partial cover (F3, F4, F5), but we also try the conceptually attractive idea of an area-weighted average of D_{84} for sediment cover and a different, lower, topographic roughness height for exposed bedrock [*Johnson*, 2014]. In reach F2 there is no sediment so a bedrock roughness height is the only option. We quantify it as s_z using fieldwork done by *Hodge and Hoey* [2016] in preparation for flume experiments in a scale model of reach F5. Most of the 80% of bare rock in F5 is exposed during low flow, and *Hodge and Hoey* [2016] constructed a high-resolution digital elevation model of an 18 m × 9 m part of it from laser scans supplemented by dGPS measurements in submerged areas. After removing the mean streamwise gradient they calculated s_z for all possible square windows of side length L in the range <1 to 9 m, thus generating statistical distributions of s_z for each window size.

For present purposes, this analysis was repeated with sediment-covered parts of the area masked out The mean value of s_z turned out to be highly scale-dependent for $L < 3$ m and still somewhat scale-dependent beyond that, increasing from ~0.06 m at $L = 3$ m to ~0.10 m at $L = 9$ m. An alternative detrending method in which a best-fit plane was subtracted from the DEM within each individual window gave slightly lower mean values of s_z, increasing from ~0.05 m to ~0.07 m for $L = 3$ to 9 m. Faced with this range of possible values of s_z we adopted a midrange value, 0.075 m, for comparison with resistance equations. Any choice within the possible range has the effect that the composite roughness height in F3–F5 is smaller than the local D_{84}, allowing us to discover whether this improves the fit of standard equations to the field data.

5. Results

5.1. Hydraulic Geometry

The trends in reach-averaged flow width, depth, velocity and Froude number as discharge increases in each reach are shown in Figure 3. In these AHG plots and subsequent diagrams, we distinguish values obtained by direct measurements at low to moderate discharges (unconnected points) from those calculated for higher discharges using the stage rating curves and EA discharge record (connected points).

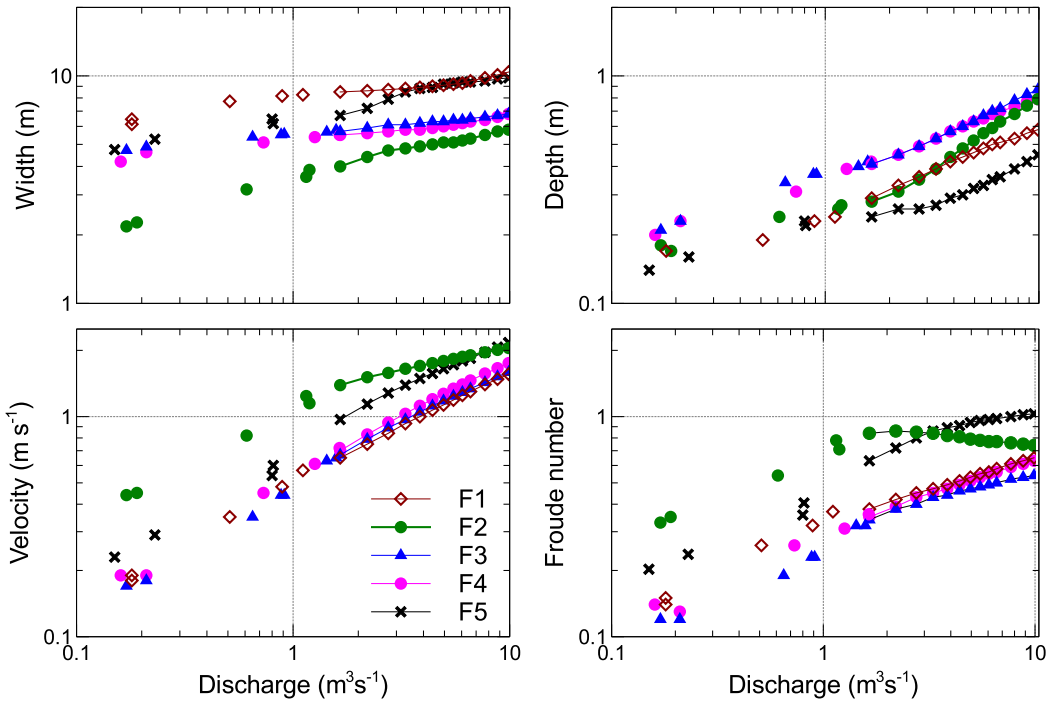

Figure 3. Hydraulic geometry of Trout Beck reaches F1–F5.

Four qualitative features are apparent in these plots. First, depth increases more rapidly with discharge than does width. This is a consequence of the channel geometry: width cannot increase rapidly with depth because there are steep side walls on both sides of the bedrock gorge (reaches F2, F3, F4) and near-vertical alluvial banks on the right side of F1 and left side of F5. However, this is not a unique feature of bedrock channels: alluvial channels with steep banks also have a lower width exponent than depth exponent.

The second feature is more distinctive. At low to moderate discharges velocity increases more rapidly with discharge than mean depth does in all five reaches. Power laws fitted to the unconnected data points in Figure 3 have exponents in the range 0.53–0.60 for velocity compared to 0.20–0.33 for depth. This implies that Manning's n decreases, because if it was constant the velocity exponent would necessarily be smaller than the depth exponent (e.g., 0.4 and 0.6, respectively, in a wide rectangular channel). This finding is consistent with studies of small steep alluvial channels with step-pool or cascade morphology; for example, *David et al*. [2010] found mean exponents of 0.39 for depth and 0.49 for velocity. With velocity increasing faster than depth, there is also a rapid increase in mean Froude number.

Third, while some of the 15 curves in Figure 3 are almost straight, indicating power law AHG behaviour, many are not. In particular, most of the depth curves are concave upwards with the corresponding velocity curves slightly convex upwards. This reflects a change in the relative rates of increase of depth and velocity. As just noted velocity increases much faster than depth at low to moderate discharge, implying a rapid reduction in n, but at higher discharges depth and velocity increase at more nearly the same rate in the four reaches with full or partial sediment cover, with depth exponents of 0.36–0.43 compared to 0.40–0.51 for velocity. This still implies a continued reduction in n. The Froude number continues to increase but more slowly, and the bulk flow only becomes critical in one reach: F5, which is relatively wider and shallow. There are nevertheless many local standing waves and hydraulic jumps in each reach.

Finally, while the curves for the bedrock reaches with extensive sediment cover (F3 and F4) do not differ in any obvious way from those for the fully alluvial reach (F1), the sediment-free bedrock reach (F2) stands out as different. It has by far the highest velocity and Froude number at low discharges, with the bulk flow close to critical at 2–3 $m^3\ s^{-1}$, but at higher discharges it has a high depth exponent (0.61) and a low velocity exponent (0.21) so that in flood conditions its velocity is no longer much higher than elsewhere and the Froude number declines slightly. Reach F5, which has much more exposed bedrock than sediment cover, also has relatively high velocity at low discharges and a relatively slow increase in velocity at high discharges.

5.2. Variation of Flow Resistance With Discharge

The AHG plots of Figure 3 indicated differences in behavior between reaches but with the common factor of a steep increase in velocity from low to moderate discharge, which implies a rapid reduction in flow resistance. These inferences are confirmed in Figure 4, which shows a strong decrease in n and f from low to moderate flows in all five reaches and a corresponding increase in $(8/f)^{1/2}$. At the lowest measured discharges n exceeds 0.1 in all four of the reaches with full or partial sediment cover, but by 2 $m^3\ s^{-1}$ it is down to 0.05–0.07 in F1, F4, and F5 although still about 0.1 in F3. The decrease in n and f, and increase in $(8/f)^{1/2}$, continues right up to the highest observed discharge in these four reaches, though the curves become less steep and n becomes almost constant in some reaches. The bare-rock gorge (F2) shows a different and unusual pattern, with a slight increase in n and f at discharges above 2 $m^3\ s^{-1}$ and a corresponding decrease in $(8/f)^{1/2}$.

Over the full range of discharge shown in Figure 4, n decreases by 60–70% in all reaches except F2, and the corresponding changes in f and $(8/f)^{1/2}$ are even larger: f decreases by over 90% and $(8/f)^{1/2}$ increases by a factor of 3–6. Part of the reason for the rapid reductions in n and f from low to moderate discharge is that they are calculated from cross-section mean velocity. Marginal dead zones are fairly extensive at these discharges in reaches F2 and F3, and locally present elsewhere, so the resistance to the active midchannel flow is less than indicated in Figure 4. However, even after allowing for dead zones there would still be a substantial decrease in central-thread flow resistance over this range of discharge. The decrease in reach-average n and f continues throughout the range of higher flows that are relevant to bed load transport. Our tracer-pebble experiment [*Ferguson et al.*, 2017] showed that significant entrainment of coarse sediment commences at 4–5 $m^3\ s^{-1}$. The only resistance coefficient that remains almost constant above this

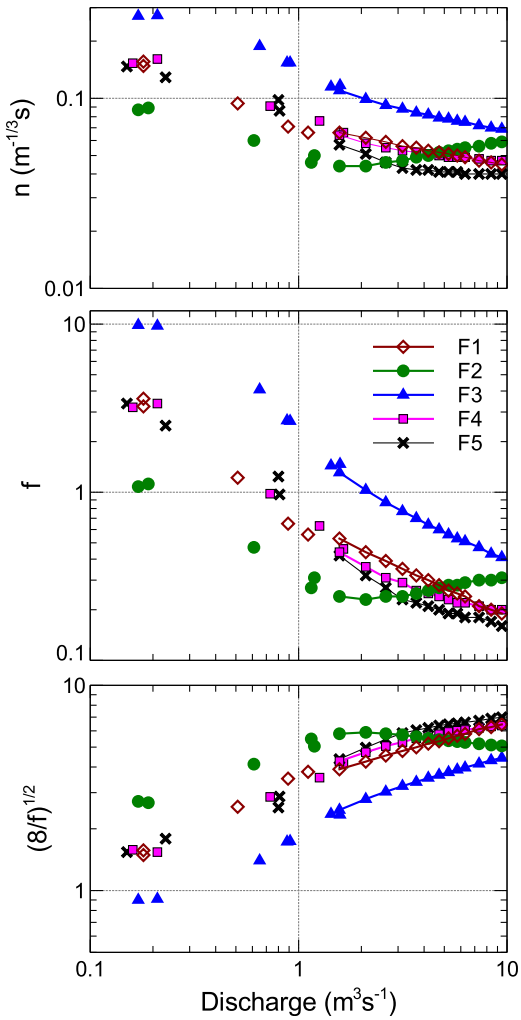

Figure 4. Variation of reach-average flow resistance with discharge in reaches F1–F5.

threshold is *n* in reaches F4 and F5. In F1 and F3 *n* decreases by 13–14%, and in all four of these reaches *f* decreases substantially (by 17–31%) and $(8/f)^{1/2}$ increases appreciably (by 10–21%).

The anomalous increase in resistance at high flows in the bare-rock reach F2 is explained by a contrast in roughness between bed and sidewalls. As can be seen in Figure 1 the limestone bed of F2 is notably smooth and in places has a channel-in-channel morphology, but the walls have large (~0.5 m amplitude) angular protrusions with intervening embayments. As flow increases from low to moderate it spreads as far as the base of the irregular side walls, with a decrease in resistance as depth increases, but above ~1.5 $m^3\ s^{-1}$ water starts to rise up the walls and dead zones develop in the embayments. F2 is narrow and its walls are high, so as discharge increases they make up an increasingly significant part of the wetted perimeter and exert progressively more form drag. This also explains the anomalous AHG curves for this reach in Figure 3. If the walls were as smooth as the bed, *n* would presumably continue to decline to below 0.04 in flood conditions rather than increase.

Since reaches F3, F4, and F5 also contain exposed rock, why do they not also experience this increase in flow resistance at high discharges? Part of the answer is that the rock sidewalls become gradually lower and less angular from F2 to F3 to F4, and the bed also becomes gradually wider, so wall drag is decreasingly important to overall resistance. Also, F3 and F4 have 70% sediment cover and that cover is coarse, so there is much less difference in roughness between bed and banks than in F2. F5 is different again in having exposed rock only in its bed, though extending almost to the top of the right bank.

The evidence from all five reaches in Trout Beck, then, is that all of the standard flow resistance coefficients vary greatly with discharge. We discuss later how this discharge dependence translates to error when predicting shear stress from discharge, or discharge from depth, on the incorrect assumption of constant *n* or constant *f*.

5.3. Spatial Differences in Flow Resistance

Figure 4 also shows systematic differences in flow resistance between reaches. The *n*-*Q* curves for the fully alluvial reach F1 and partial-cover reaches F3, F4 and F5 all have approximately the same shape but they are shifted vertically in the plots. The same is true if resistance is quantified by *f* or $(8/f)^{1/2}$. At any given discharge F3 has much higher flow resistance than F1 and F4, which in turn have slightly higher resistance than F5 at all but the lowest discharges. The sediment-free reach F2 has by far the lowest resistance of all at low discharges, but the increase in resistance once flow rises up its irregular walls takes it above F1, F3, and F4 by 5 $m^3\ s^{-1}$ and to almost as high a resistance as F3 at the highest discharges.

In explaining the anomalous behavior of F2, we recognized that some parts of the wetted perimeter are rougher than others. The same is true in the other reaches, though in different ways and to varying extent. The fully alluvial channel (F1) is the most homogeneous, since it is relatively wide and its alluvial banks are not notably smoother or rougher than its bed. The other three reaches all have some exposed bedrock. In F3 and F4 the rock bed is smooth, as in F2, but 70% of it is covered by sediment which in these reaches is

much coarser than in F1 (Table 1). The mixture of smooth rock and coarse sediment in F4 gives almost the same overall flow resistance as in F1 with its complete, but finer, sediment cover. F3 has considerably higher resistance than F4 despite a similar cover percentage and D_{84}; the main difference is that F3 has a far higher boulder density than any other reach (Table 1). The boulders are immobile in all but extreme floods, protrude above the water surface at low to moderate discharges, and extract momentum from the flow through form drag and spill losses. F5 is different in having no vertical rock walls and only 20% sediment cover, most of it in the thalweg. The exposed rock in its bed has a smooth but fissured surface with a slight lateral tilt (see Figure 1). It becomes progressively inundated at higher discharges, when this reach has the lowest resistance of all. The implication is that the effective roughness of the rock bed in F5 is lower than that of the sediment in F1.

In summary, some parts of the bedrock channel have higher flow resistance than the upstream alluvial channel while others have lower resistance. The lowest resistance is where flow is mainly over a relatively smooth bedrock floor; the highest resistance is where flow is mainly over a very coarse sediment cover.

6. Discussion

Our finding that n and f decrease, and $(8/f)^{1/2}$ increases, with increasing discharge in the partial-cover reaches of Trout Beck is consistent with what little evidence there is from previous field measurements of resistance at multiple stages in bedrock reaches [*Heritage et al.*, 2004; *Richardson and Carling*, 2006]. A strong decrease in resistance with increasing discharge is also normal in small steep alluvial streams with coarse beds [e.g., *Lee and Ferguson*, 2002; *Ferguson*, 2007; *Reid and Hickin*, 2008; *Rickenmann and Recking*, 2011; *Nitsche et al.*, 2012; *D'Agostino and Michelini*, 2015], and it is not surprising that bedrock channels with extensive coarse sediment cover behave similarly.

In view of these findings, we consider in section 6.1 how the Trout Beck results compare with traditional and alternative resistance laws for coarse alluvial channels. Section 6.2 then considers the implications of the results for incision models and paleoflood estimation and discusses how stage-dependent n and f could be allowed for in those applications.

6.1. Comparison With Resistance Laws for Alluvial Channels

Almost all well-known flow resistance laws can be written as equations predicting $(8/f)^{1/2}$ from the relative submergence of the bed, commonly quantified by R/D_{84} in alluvial channels but more generally by R/k where k is a roughness height. Figure 5a shows the Trout Beck data plotted using sediment D_{84} as the roughness height, with no allowance for the lower roughness of exposed bedrock. Reach F2 is excluded from this plot since it contains no sediment. For comparison, Figure 5b uses roughness heights calculated as an area-weighted average of D_{84} for the sediment cover and the previously explained (section 4.3) value of 0.075 m for exposed bedrock. Also shown in Figure 5 are the upper and lower bounds of measured resistance in the biggest alluvial-channel data compilation known to us [*Rickenmann and Recking*, 2011], and curves for three well-known prediction equations from the literature: Manning-Strickler (equation (1) above with $n = D_{84}^{1/6}/a_1 g$ and $a_1 = 6.5$), the logarithmic equation (equation (3)) with $k = 3.5D_{84}$ as proposed for gravel-bed rivers by *Hey* [1979], and the VPE (equation (5)) with $a_1 = 6.5$ and $a_2 = 2.5$ as suggested in *Ferguson* [2007]. The 0.6-power relation proposed by *Rickenmann* [1991] is very close to the lower end of the VPE curve so is not shown separately.

Comparison of Figures 5a and 5b shows that reaches F1, F4, and F5 plot well apart when using D_{84} as roughness height but close together when using the area-weighted average of sediment and rock roughness. At moderate discharges the bedrock reach F2 also plots close to F1, F4, and F5 in Figure 5b, though at higher discharges its irregular walls cause the anomalous increase in resistance that was discussed in relation to Figure 4. This tendency for alluvial, bedrock and mixed reaches to collapse to a common trend at relative submergences of 2–4, where macroroughness is starting to become important, supports the use of the hybrid-roughness approach. However, the boulder-riffle reach F3 plots well below the other reaches in Figure 5a and even farther below in Figure 5b, where it plots at the limit of the observed range of alluvial flow resistance. For F3 to fall into line with the other reaches its sediment roughness height would have to be much larger than the measured D_{84} of 190 mm. The high density of boulders in this reach may be relevant, since resistance in this reach must be due mainly to form drag and therefore depends on the shapes,

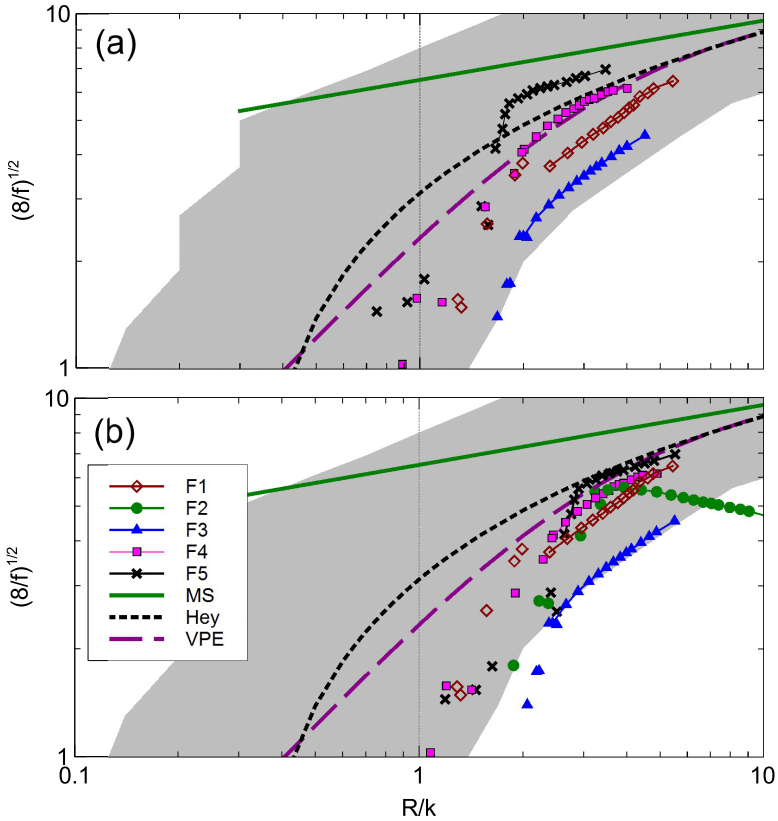

Figure 5. Relation of flow resistance to relative submergence in reaches F1–F5, with roughness height k taken as (a) sediment D_{84} or (b) an area-weighted average of sediment D_{84} and bedrock s_z. MS, Hey, and VPE denote the Manning-Strickler, *Hey* [1979] and variable-power [*Ferguson*, 2007] prediction equations. Gray shading shows envelope of 2890 alluvial-channel data points compiled by *Rickenmann and Recking* [2011].

frontal areas, density, and arrangement of large clasts as well as their average size [e.g., *Bathurst*, 1978; *Yager et al.*, 2007]. *Nitsche et al.* [2012] found that flow resistance in six steep cobble-boulder channels increased with areal boulder density over and above the effect of D_{84}, and boulders sitting on bedrock might have even more effect if they have greater frontal area than similar-sized clasts embedded in gravel and cobbles.

In both versions of Figure 5, it is apparent that the Manning-Strickler equation performs badly in Trout Beck, overestimating $(8/f)^{1/2}$ even in flood conditions and drastically so at lower discharges. The assumption that n has a fixed value that depends on local grain size is also inconsistent with the strong discharge dependence of the measured n values (Figure 4), and the Strickler n values of 0.027–0.030 for the Trout Beck reaches are far lower than the measured values even at high discharges. The Manning equation with n estimated from R and S using *Jarrett*'s [1984] equation cannot be shown in Figure 5 because it does not use a bed grain size, but calculations show that it performs quite well in the boulder-riffle reach F3. As might be expected it drastically underestimates velocities at all discharges in F2 (100% bedrock) and F5 (80% bedrock). It also underestimates velocities in F1 and F4, and underestimates the extent to which n changes with discharge in all reaches.

The convex-up trends of the data from the four fully or partly sediment-covered reaches are better captured by *Hey*'s [1979] logarithmic law or the VPE. However, both of these equations greatly underestimate the measured flow resistance in F3 at all discharges and somewhat underestimate resistance in all reaches at low discharges when the relative submergence is around 1. Here the trend of the data appears to be even steeper than the $(8/f)^{1/2} \propto R/k$ that was proposed by *Rickenmann* [2001] and *Aberle and Smart* [2003] and forms the asymptote of the VPE.

The Trout Beck data are compared in Figure 6 with the nondimensional AHG of *Rickenmann and Recking* [2011], which used $k = D_{84}$ as the roughness height in a relation between v^{**} and q^{**} for coarse-bed alluvial

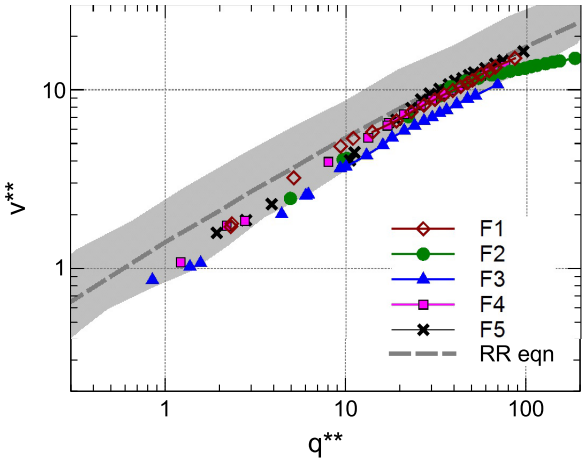

Figure 6. Nondimensional hydraulic geometry plot of Trout Beck measurements using variables q^{**} and v^{**} defined in section 2.5. Gray shading shows envelope of *Rickenmann and Recking*'s [2011] alluvial-channel data and "RR eqn" denotes their equation (22).

channels. As in Figure 5b, we estimate k as the area-weighted average of D_{84} for sediment and 0.075 m for exposed bedrock. The measurements in the alluvial reach (F1) and two of the partial cover reaches (F4 and F5) plot close to *Rickenmann and Recking*'s [2011] equivalent of the VPE prediction equation, as does the bedrock gorge (F2) at moderate discharges, but the boulder riffle (F3) plots near the lower (high resistance) limit of alluvial-channel data. As before, the effective roughness height in F3 would have to nearly twice the D_{84} diameter to bring this reach into line with the general trend. This again suggests that the measured D_{84} is an inadequate proxy for the hydraulic roughness of a boulder-rich sediment cover.

6.2. Implications

Our results show a strong decrease in n and f as discharge increases (Figure 4), apart from the effects of rough walls in F2. If other bedrock channels behave similarly there may be implications for models of incision processes and landscape evolution, since as discussed in section 2.4 many of them calculate depth and shear stress from discharge on the assumption of constant n or constant f. To obtain some idea of how sensitive this calculation is, consider the simple case of a rectangular channel of fixed gradient and neglect the difference between d and R. Then $\tau \propto d \propto Q^{0.60}$ if Manning's n is assumed constant, or $\tau \propto Q^{0.67}$ if f is assumed constant. Even when attention is restricted to discharges competent to move sediment ($Q \geq 4$ m^3 s^{-1}), our data show n varying as $Q^{0.20}$ in F2 and as $Q^{-0.06}$ to $Q^{-0.20}$ in the other reaches. Applying this range of behavior to our hypothetical channel gives τ-Q relations with exponents anywhere between 0.48 and 0.72, instead of 0.60 or 0.67 as implied by fixed n or fixed f. Whether this has a significant effect on the main conclusions from modeling exercises is beyond the scope of the present paper, but modelers could investigate it by comparing results for fixed n or f with those using stage-varying resistance. We speculate that the sensitivity might be greater in models that allow for stochastic variation in flood discharges as urged by *Lague et al.* [2005].

This raises two questions: which alternative assumptions about flow resistance in bedrock channels might be more realistic, and how they could be implemented in incision models? We showed above that either a logarithmic or a variable-power dependence on relative submergence is more realistic than fixed n in the partial-cover reaches of Trout Beck. Direct calculation of shear stress from discharge using these laws requires iterative calculations, but in the nondimensional hydraulic geometry approach depth can be calculated explicitly as $d = k{\cdot}q^{**}/v^{**}$, with v^{**} estimated from q^{**} using equation (22) of *Rickenmann and Recking* [2011]. These approaches implicitly calculate stage-varying values of n and f from a user-specified roughness length scale.

The potential for error in paleoflood estimation differs from that in incision modeling because a known depth is used to estimate an unknown discharge, rather than the other way round. If a fixed value of n is assumed, the estimated discharge is inversely proportional to it, with scope for large errors if the n value applicable to the paleoflood is overestimated or underestimated. In narrow gorges with deep flood flows it may be that n is more or less constant over a wide range of high discharges, but the problem remains of deciding its value. Overestimation of n, with consequent underestimation of paleodischarge, is a strong possibility if flow measurements at a low discharge are used to calculate n and the same value is extrapolated to flood conditions. One way to allow for the stage dependence of n in such circumstances would be to use the low-flow measurement to calibrate the roughness height in the logarithmic law or VPE and use that law to calculate v, and thus n, at the known paleoflood depth. In the absence of any flow measurements at all, the value of n has to be estimated in some way. As noted by *Miller and Cluer* [1998] and demonstrated quantitatively by *Wohl* [1998] this introduces substantial uncertainty in the paleoflood estimate. If bed grain

size measurements are available the logarithmic and VPE laws could be used to obtain additional estimates of paleoflood *n* to inform the choice.

A complication relevant to both types of application is the possibility of different effective roughness heights in different parts of the wetted perimeter. *Johnson* [2014] allowed for such a difference by using an area-weighted average, and we showed in Figure 5b that this averaging approach improves the collapse of the Trout Beck data. Johnson noted that in principle a third value could be used for wall roughness, which would clearly be helpful in our F2 reach and might be relevant to paleoflood estimation in rock gorges with irregular walls. Calculations with different bed and wall roughness would be easier to implement in paleoflood estimation, where depth is known, than in incision models where depth is the desired solution and iterative calculations would be required. In either case the difficulty remains of how to quantify the wall roughness and its effect on bulk flow. One possibility is some metric of the topographic irregularity of the walls, as suggested by *Kean and Smith* [2006].

7. Conclusions

Our measurements and calculations of bulk hydraulic properties of five reaches of Trout Beck over a wide range of discharge lead to several conclusions that have wider implications.

1. First, neither of the standard resistance coefficients *n* and *f* is invariant with discharge in any reach, whether the bed is entirely bedrock, entirely alluvial, or a mixture. Instead, *n* and *f* decrease rapidly from low to moderate flow, and with one exception continue to decrease more slowly in moderate flood conditions. If this finding holds for bedrock channels generally it has implications for models of bedrock incision processes, paleoflood reconstruction when measurements of *n* exist only for low discharges if at all, and engineering calculations.
2. The sediment-free bedrock reach in Trout Beck is abnormal in experiencing an increase in flow resistance from medium to high discharge, which we explain as due to the walls being far rougher than the bed. This exception to conclusion (1) raises a second factor that is potentially relevant to incision modeling of, or paleoflood reconstruction in, narrow channels. Differences between rivers in wall roughness lead to differences in overall flow resistance and also in how resistance changes with discharge. A single roughness coefficient cannot capture the stage dependence correctly in this situation.
3. Spatial differences in bulk flow resistance along our study stream are due to a combination of factors: differences in the proportion of exposed rock in the bed, in the coarseness of the sediment cover, and in the character of the walls. Resistance is fairly high to very high in all reaches at all discharges, but the smoothness of the exposed bedrock means that reaches with less sediment cover have lower overall resistance. The opposite might occur in a channel with transverse rock ribs [*Goode and Wohl*, 2010]. Again, a composite calculation using different roughness lengths is desirable in such situations and would allow flow resistance to vary over time in models that allow sediment cover to vary [e.g., *Johnson*, 2014].
4. Not only does a fixed value of Manning's *n* fail to capture the stage dependence of flow resistance, but if *n* is estimated from bed grain size using a Strickler-type relation the flow resistance is drastically underestimated, particularly (but not only) when discharge is low. This is because equating roughness height with grain size in this way neglects the form drag on large, protruding and possibly immobile clasts or clast structures. We suspect this finding applies to most bedrock channels, since boulders are commonly present as a result of plucking and sidewall collapse.
5. Logarithmic and variable-power flow resistance laws give a better fit than Manning-Strickler to our results. This is consistent with what has been found for coarse-bed alluvial rivers [e.g., *Ferguson*, 2007; *Rickenmann and Recking*, 2011]. However, the goodness of fit of the logarithmic and VPE laws is sensitive to the specification of roughness height. In the present case, using an area-weighted average of sediment D_{84} and bedrock s_z gives fairly consistent predictions for three reaches, and for moderate flows in the sediment-free reach, but seriously under-predicts resistance in a reach with little exposed bedrock and many boulders. Comparative tests of alternatives to D_{84} would be useful.

If future researchers want to allow for discharge-dependent flow resistance in bedrock channels, we suggest that a convenient way to predict depth and shear stress from discharge is to use the nondimensional hydraulic geometry approach of *Rickenmann and Recking* [2011], though not necessarily with D_{84} as

roughness height. For estimating paleoflood discharge from depth, logarithmic or variable-power resistance laws can be used though again with due consideration to how roughness is specified.

Finally, knowledge of the bulk hydraulics of bedrock channels remains very limited. Hydraulic measurements over a range of discharges need to be made in other bedrock channels, preferably including larger and deeper channels and those with rougher bedrock floors, in order to test how widely applicable our findings are. They could usefully be combined with investigations of how best to quantify the effective roughness height of exposed rock floors and walls.

Acknowledgments
This research was supported by a Durham University doctoral studentship to BPS, with additional fieldwork funding from a British Society for Geomorphology small grant. Fieldwork was done by BPS with assistance from the other authors, technician Chris Longley, and numerous student helpers. All authors contributed to planning the project, interpreting the results, and refining the paper, which was drafted by RIF. The bulk hydraulic results are available on request from RIF (r.i.ferguson@durham.ac.uk) or JW (jeff.warburton@durham.ac.uk) on condition that we are acknowledged in any subsequent publication. We thank three anonymous reviewers for constructive comments.

References

Aberle, J., and G. M. Smart (2003), The influence of roughness structure on flow resistance on steep slopes, *J. Hydraul. Res.*, *41*, 259–269.
Barnes, H. H. (1967), Roughness characteristics of natural channels, *U.S. Geol. Surv. Water-Supply Pap*. 1849, U.S. Govt. Printing Office, Washington, D. C.
Bathurst, J. C. (1978), Flow resistance of large-scale roughness, *J. Hydraul. Div. Am. Soc. Civ. Eng.*, *104*, 1587–1603.
Benito, G., and V. R. Thorndycraft (2005), Palaeoflood hydrology and its role in applied hydrological sciences, *J. Hydrol.*, *313*, 3–15.
Chatanantavet, P., and G. Parker (2008), Experimental study of bedrock channel alluviation under varied sediment supply and hydraulic conditions, *Water Resour. Res.*, *44*, W12446, doi:10.1029/2007WR006581.
Chatanantavet, P., and G. Parker (2009), Physically based modeling of bedrock incision by abrasion, plucking, and macroabrasion, *J. Geophys. Res.*, *114*, F04018, doi:10.1002/2008JF001044.
Chow, V. T. (1959), *Open-Channel Hydraulics*, McGraw-Hill, New York.
D'Agostino, V., and T. Michelini (2015), On kinematics and flow velocity prediction in step-pool channels, *Water Resour. Res.*, *51*, 4650–4667, doi:10.1002/2014WR016631.
David, G. C., E. Wohl, S. E. Yochum, and B. P. Bledsoe (2010), Controls on at-a-station hydraulic geometry in steep headwater streams, Colorado, USA, *Earth Surf. Processes Landforms*, *35*, 1820–1837.
David, G. C. L., E. Wohl, S. E. Yochum, and B. P. Bledsoe (2011), Comparative analysis of bed resistance partitioning in high-gradient streams, *Water Resour. Res.*, *47*, W07507, doi:10.1029/2010WR009540.
Dingman, S. L. (2007), Analytical derivation of at-a-station hydraulic-geometry relations, *J. Hydrol.*, *334*, 17–27.
Ferguson, R. (2007), Flow resistance equations for gravel- and boulder-bed streams, *Water Resour. Res.*, *43*, W05427, doi:10.1029/2006WR005422.
Ferguson, R. (2013), Reach-scale flow resistance, In *Treatise on Geomorphology, Fluvial Geomorphol.*, vol. 9, edited by J. Schroder and E. Wohl, pp. 50–68, Elsevier, San Diego, Calif.
Ferguson, R. I. (1986), Hydraulics and hydraulic geometry, *Prog. Phys. Geogr.*, *10*, 1–31.
Ferguson, R. I., B. P. Sharma, R. A. Hodge, R. J. Hardy, and J. Warburton (2017), Bedload tracer mobility in a mixed bedrock/alluvial channel, *J. Geophys. Res. Earth Surf.*, *122*, doi:10.1002/2016JF003946.
Gleason, C. J. (2014), Hydraulic geometry of natural rivers: A review and future directions, *Prog. Phys. Geog.*, *39*(3), 337–360.
Goode, J. R., and E. Wohl (2010), Substrate controls on the longitudinal profile of bedrock channels: Implications for reach-scale roughness, *J. Geophys. Res. Earth Surf.*, *115*, F03018, doi:10.1029/2008JF001188.
Heritage, G. L., B. P. Moon, L. J. Broadhurst, and C. S. James (2004), The frictional resistance characteristics of a bedrock-influenced river channel, *Earth Surf. Processes Landforms*, *29*, 611–627.
Hey, R. D. (1979), Flow resistance in gravel-bed rivers, *J. Hydraul. Div. Am. Soc. Civ. Eng.*, *105*(HY9), 365–379.
Hodge, R. A., and T. B. Hoey (2016), A Froude-scaled model of a bedrock-alluvial channel reach: 1. Hydraulics, *J. Geophys. Res. Earth Surf.*, *121*, 1578–1596, doi:10.1002/2015JF003706.
Howard, A. D. (1994), A detachment-limited model of drainage basin evolution, *Water Resour. Res.*, *30*, 2261–2285.
Inoue, T., N. Izumi, Y. Shimizu, and G. Parker (2014), Interaction among alluvial cover, bed roughness, and incision rate in purely bedrock and alluvial-bedrock channel, *J. Geophys. Res. Earth Surf.*, *119*, F03018, doi:10.1002/2014JF003133.
Inoue, T., T. Iwasaki, G. Parker, Y. Shimizu, N. Izumi, C. P. Stark, and J. Funaki (2016), Numerical simulation of effects of sediment supply on bedrock channel morphology, *J. Hydraul. Eng.*, *142*(7), 04016014,
Jarrett, R. D. (1984), Hydraulics of high-gradient rivers, *J. Hydraul. Eng.*, *110*, 1519–1539
Johnson, J. P. (2014), A surface roughness model for predicting alluvial cover and bedload transport rate in bedrock channels, *J. Geophys. Res. Earth Surf.*, *119*, 2147–2173, doi:10.1002/2013JF003000.
Kean, J. W., and J. D. Smith (2006), Form drag in rivers due to small-scale natural topographic features: 2. Irregular sequences, *J. Geophys. Res. Earth Surf.*, *111*, F04010, doi:10.1029/2006JF00049.
Keulegan, G. H. (1938), Laws of turbulent flow in open channels, *J. Res. Natl. Bur. Stand.*, *21*, 707–741.
Kidson, R. L., K. S. Richards, and P. A. Carling (2006), Hydraulic model calibration for extreme floods in bedrock-confined channels: Case study from northern Thailand, *Hydrol. Processes*, *20*, 329–344.
Lague, D., N. Hovius, and P. Davy (2005), Discharge, discharge variability, and the bedrock channel profile, *J. Geophys. Res.*, *110*, F04006, doi:10.1029/2004/F000259.
Lamb, M. P., W. E. Dietrich, and L. S. Sklar (2008), A model for fluvial bedrock incision by impacting suspended and bed load sediment, *J. Geophys. Res.*, *113*, F03025, doi:10.1029/2007JF000915.
Lee, A. J., and R. I. Ferguson (2002), Velocity and flow resistance in step-pool streams. *Geomorphology*, *46*, 59–71.
Leopold, L. B., and T. Maddock (1953), Hydraulic geometry of stream channels and some physiographic implications, *U.S. Geol. Surv. Prof. Pap.*, *272*, 57 pp., U.S. Govt. Printing Office, Washington, D. C.
Miller, A. J., and B. L. Cluer (1998), Modeling considerations for simulation of flow in bedrock channels, in *Rivers over Rock: Fluvial Processes in Bedrock Channels, Geophys. Monogr.*, vol. 107 edited by K. J. Tinkler and E. E. Wohl, pp. 61–104, AGU, Washington, D. C.
Nelson, P. A., and G. Seminara (2012), A theoretical framework for the morphodynamics of bedrock channels, *Geophys. Res. Lett.*, *39*, L06408, doi:10/1029/2011GL050806.
Nitsche, M., D. Rickenmann, J. W. Kirchner, J. M. Turowski, and A. Badoux (2012), Macroroughness and variations in reach-averaged flow resistance in steep mountain streams, *Water Resour. Res.*, *48*, W12518, doi:10.1029/2012WR012091.

O'Connor, J. B., and R. H. Webb (1988), Hydraulic modeling for paleoflood analysis, in *Flood Geomorphology*, edited by V. R. Baker, R. C. Kochel and P. C. Patton, pp. 393–402, Wiley New York.
Powell, D. M. (2015), Flow resistance in gravel-bed rivers: Progress in research, *Earth Sci. Rev.*, *136*, 301–338.
Reid, D. E., and E. J. Hickin (2008), Flow resistance in steep mountain streams, *Earth Surf. Processes Landforms*, *33*, 2211–2240.
Richardson, K., and P. A. Carling (2006), The hydraulics of a straight bedrock channel: Insights from solute dispersion studies, *Geomorphology*, *82*, 98–125.
Rickenmann, D. (1991), Hyperconcentrated flow and sediment transport at steep slopes, *J. Hydraul. Div. Am. Soc. Civ. Eng.*, *117*, 1419–1439.
Rickenmann, D., and A. Recking (2011), Evaluation of flow resistance equations using a large field data base, *Water Resour. Res.*, *47*, W07538, doi:10.1029/2010WR009793.
Siddiqui, A., and A. Robert (2010), Thresholds of erosion and sediment movement in bedrock channels, *Geomorphology*, *118*, 301–313.
Smart, G. M., M. J. Duncan, and J. M. Walsh (2002), Relatively rough flow resistance equations, *J. Hydraul. Eng.*, *128*, 568–578.
Strickler, A. (1923), *Beitrage zur Frage der Geschwindigkeitsformel unbd der Rauhigkeitszahlen für Ströme, kanäle, und geschlossene Laitungen*, 77 pp., Mitteilungen Nr.16 des Amtes für Wasserwirtschaft, Eidgenössisches Departement des Innern, Bern.
Turowski, J. M., D. Lague, and N. Hovius (2007), Cover effect in bedrock abrasion: A new derivation and its implications for the modeling of bedrock channel morphology, *J. Geophys. Res.*, *112*, F04006, doi:10.1029/2006JF000697.
Turowski, J. M., N. Hovius, A. Wilson, and M.-J. Horng (2008), Hydraulic geometry, river sediment and the definition of bedrock channels, *Geomorphology*, *99*, 26–38, doi:10.1016/j.geomorph.2007.10.001.
Turowski, J. M., N. Hovius, H. Meng-Long, D. Lague, and C. Men-Chiang (2009), Distribution of erosion across bedrock channels, *Earth Surf. Processes Landforms 33*, 353–363.
Whipple, K. X., and G. E. Tucker (1999), Dynamics of the stream-power river incision model: Implications for height limits of mountain ranges, landscape response timescales, and research needs, *J. Geophys. Res.*, *104*, 17,661–17,674.
Wohl, E. E. (1998), Uncertainty in flood estimates associated with roughness coefficient, *J. Hydraul. Div. Am. Soc. Civ. Eng.*, *124*(2), 219–223.
Yager, E. M., J. W. Kirchner, and W. E. Dietrich (2007), Calculating bed load transport in steep boulder bed channels, *Water Resour. Res.*, *43*, W07418, doi:10.1029/2006WR005432.
Zhang, L., G. Parker, C. P. Stark, T. Inoue, E. Viparelli, X. Fu, and N. Izumi (2015), Macro-roughness model of bedrock-alluvial river morphodynamics, *Earth Surf. Dyn.*, *3*, 113–138.